ELSEVIER

Contents lists available at ScienceDirect

Computational Materials Science

journal homepage: www.elsevier.com/locate/commatsci





Thermal conductivity of magnesium selenide (MgSe)–A first principles study

Rajmohan Muthaiah*, Jivtesh Garg

School of Aerospace and Mechanical Engineering, University of Oklahoma, Norman, OK 73019, USA

ARTICLE INFO

Keywords:
Density functional theory
Magnesium
Selenium
Thermal conductivity
Semiconductors

ABSTRACT

Wide bandgap semiconductor has recently attracted attraction for power electronics, thermoelectric and high temperature applications. Magnesium Selenide (MgSe) is a wide bandgap semiconductor extensively studied for its electronic, magnetic, optical and structural properties. In this work, we report the temperature and length dependence lattice thermal conductivity of magnesium selenide (MgSe) with different crystallographic phase; zincblende (ZB), rocksalt (RS), wurtzite (WZ) and nickel arsenic (NiAs) using first principles computations. Our first principles calculations results shows a low thermal conductivity of MgSe with $k_{\rm NiAs} < k_{\rm rocksalt} < k_{\rm wurtzite} < k_{\rm zincblende}$. We systematically investigated the elastic constants, phonon frequencies, phonon scattering rate and mode contribution thermal conductivity. Our first principles calculations shows a room temperature low thermal conductivity of 4.54 Wm⁻¹K⁻¹ for the NiAs phase due to the strong phonon–phonon scattering and 21.27 Wm⁻¹K⁻¹ for the zincblende structure very low phonon–phonon scattering arising from the phonon bandgap. Our results elucidate that MgSe_(NiAs) compounds with low thermal conductivity and MgSe_(ZB) with high thermal conductivity will be a promising material for thermoelectric applications and thermal management systems respectively.

1. Introduction

Wide bandgap materials have attracted various scientific and technological interest due to its reduced energy consumption, low power loss and can accommodate higher operating temperatures, high switching speed and high voltage, high frequencies [1-3] and thermoelectric applications [4–7]. Magnesium chalcogenides such as magnesium sulphide (MgS), magnesium selenide (MgSe) and magnesium telluride (MgTe) are wide bandgap semiconductors which are extensively studied for their electronic [8-10], magnetic [9], optical [8], structural [9,11-13] and vibrational [14,15] properties. Understanding thermal conductivity of these materials is critical for optimum thermal design of devices based on these materials. There are, however, limited studies on thermal properties which is critical for wide range of applications such as thermoelectrics [16-21], thermal management systems [22-27], optoelectronics [28], thermal barrier coatings [29-31] and solar cells [32–34] etc., which inspired us to compute it. In this work, we report the temperature and length dependence thermal conductivity of MgSe with different crystalline phases using first principles calculations and phonon Boltzmann transport equation. MgSe exists in four crystalline phases; zincblende (ZB), rocksalt (RS), wurtzite (WZ) and nickel arsenic (NiAs) [14]. We also report the length dependence thermal conductivity for its nanostructures. At 300 K, the first principles computed thermal conductivities of MgSe are – a) 4.54 $\rm Wm^{-1}K^{-1}$ along a-axis and 6.37 $\rm Wm^{-1}K^{-1}$ along c-axis for NiAs structure, b) 11.89 $\rm Wm^{-1}K^{-1}$ for RS structure, c) 19.58 $\rm Wm^{-1}K^{-1}$ a-axis and 20.39 $\rm Wm^{-1}K^{-1}$ along c-axis for WZ structure and d) 21.27 $\rm Wm^{-1}K^{-1}$ for ZB structure. Understanding of differences in thermal conductivity is achieved through analysis of differences in phonon scattering arising from different phonon dispersions for different structures.

2. Computational Methods:

All the first principles calculations were performed using QUANTUM ESPRESSO [35] package. Norm-conserving pseudopotential with local density approximation (LDA) [36] exchange–correlation functional is used for electronic calculations. The geometries of the ZB and RS MgSe with 2 atom unit cell and WZ and NiAs structures with 4 atom unit cell, were optimized until forces on all atoms were less than 10^{-6} Ry/bohr. Plane-wave energy cutoff of 70 Ry was used for electronic calculations.

E-mail address: rajumenr@ou.edu (R. Muthaiah).

^{*} Corresponding author.

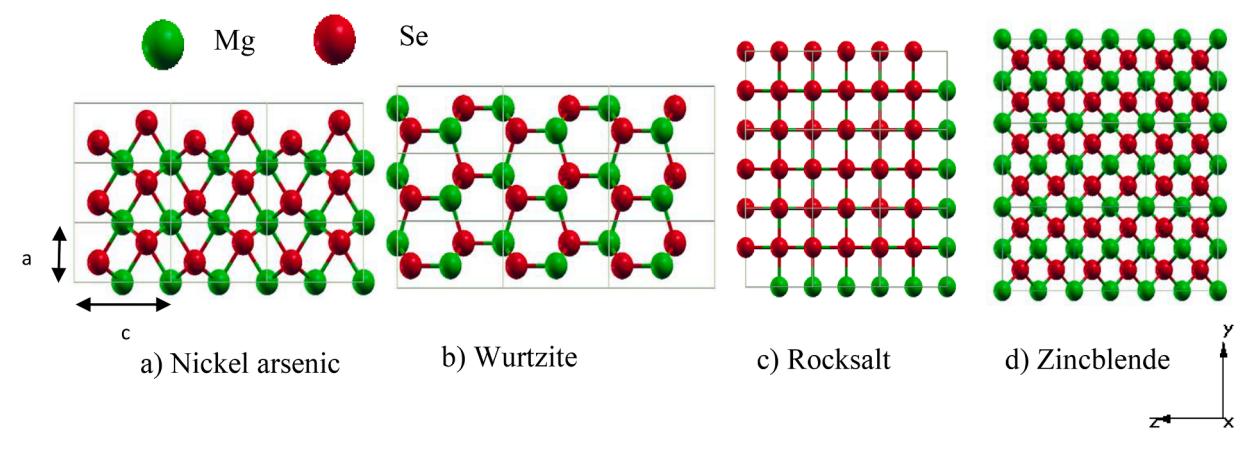


Fig. 1. (a-d): Crystal structure of MgSe with crystalline phases; NiAs (a = 7.216 bohr, c/a = 1.6672), wurtzite (a = 7.924 bohr, c/a = 1.6149), rocksalt (a = 10.2617 bohr) and zincblende (a = 11.16 bohr) respectively.

Table 1
Lattice constants, Bulk modulus (B), Youngs modulus (E), Shear modulus (G) and poisson's (v) ratio of MgSe with different crystal phase.

| S. No | Crystal phase | a (bohr) | c/a | B (GPa) | E (GPa) | G (GPa) | υ |
|-------|-----------------------|----------|-------|---------|---------|---------|--------|
| 1. | Nickel arsenic (NiAs) | 7.216 | 1.667 | 67.36 | 92.8 | 36.53 | 0.2703 |
| 2. | Wurtzite (WZ) | 7.9238 | 1.615 | 50.7 | 55.34 | 21 | 0.3182 |
| 3. | Rocksalt (RS) | 10.2617 | | 67.7 | 113.07 | 46.28 | 0.2216 |
| 4. | Zincblende (ZB) | 11.16 | | 49.695 | 47.903 | 17.933 | 0.3356 |

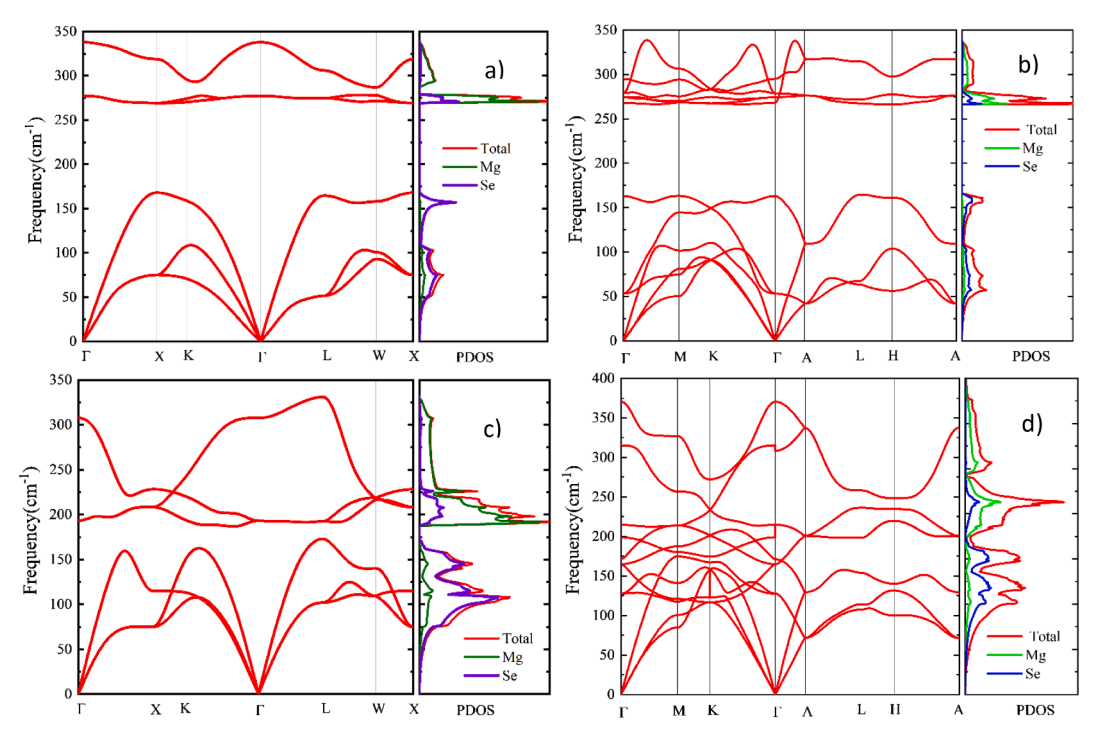


Fig. 2. Phonon dispersion and phonon density of states (PDOS) of MgSe with crystalline phase; a) ZB b) WZ c) RS and d) NiAs.

Monkhorst-Pack [37] k-point mesh sizes of $8 \times 8 \times 8$ and $12 \times 12 \times 8$ were used for ZB/RS and WZ/NiAs structures, respectively, to integrate over the Brillouin zone. Relaxed structures with equilibrium lattice constants of MgSe with different lattice crystal phases are shown in Fig. 1 and also listed in Table 1 (in excellent agreement with previously published values [10,14,38–40]).

Lattice thermal conductivity (k) was computed by solving phonon Boltzmann transport equation (PBTE) [41] in both single mode relaxation approximation (SMRT) [42] and exactly by using a variational

method. Expression for thermal conductivity (k) obtained by solving PBTE in the single mode relaxation time (SMRT) approximation is given by,

$$k_{\alpha} = \frac{\hbar^2}{N\Omega k_b T^2} \sum_{\lambda} v_{\alpha\lambda}^2 \omega_{\lambda}^2 \overline{n}_{\lambda} (\overline{n}_{\lambda} + 1) \tau_{\lambda}$$
 (1)

where, α , \hbar , N, Ω , k_b , T, are the cartesian direction, Planck constant, size of the q mesh, unit cell volume, Boltzmann constant, and absolute

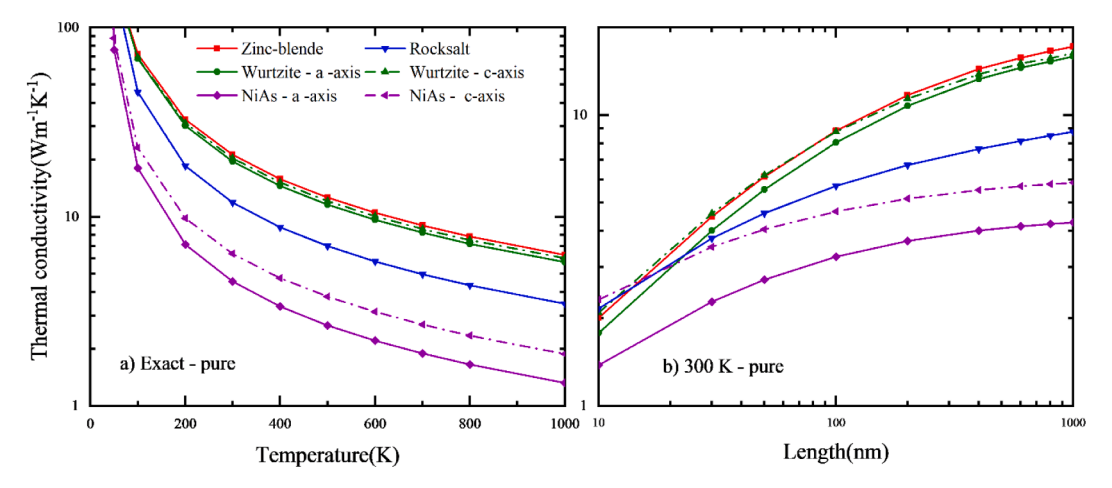


Fig. 3. Temperature dependent lattice thermal conductivity of MgSe with different crystalline phase with a) iterative solution of BTE c) Length dependent thermal conductivity of MgSe at room temperature (300 K).

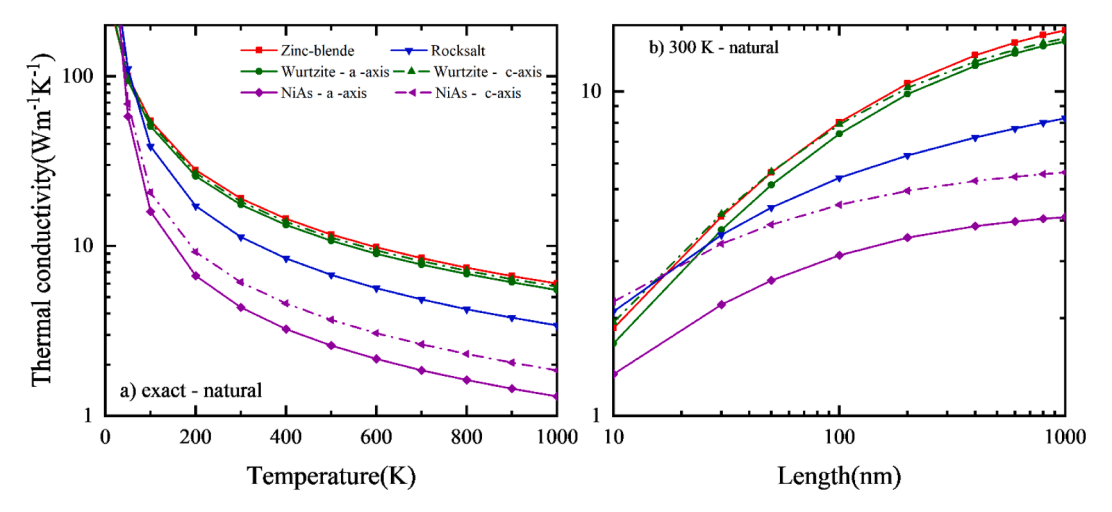


Fig. 4. (a and b) Temperature and length dependent (300 K) thermal conductivity of natural MgSe with isotopic scattering for different crystalline phase.

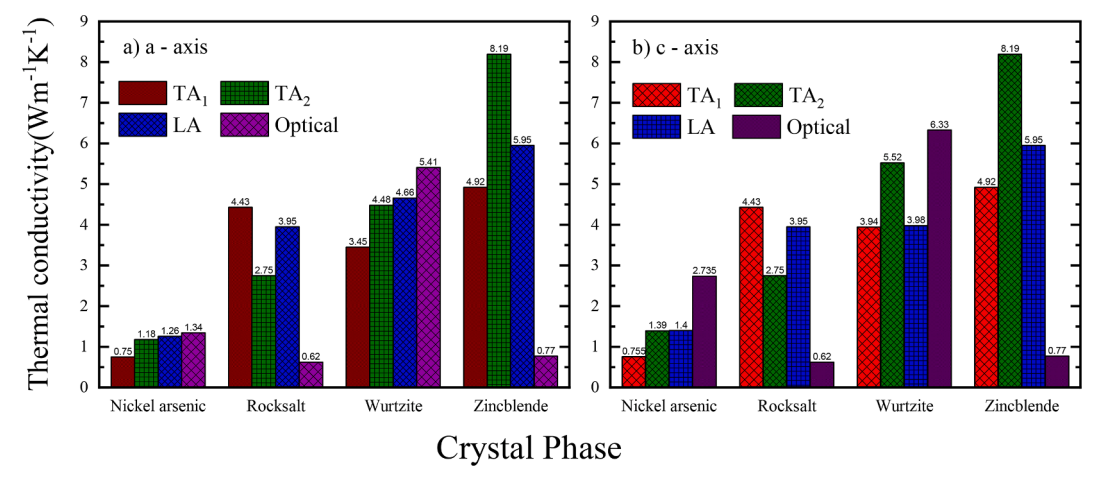
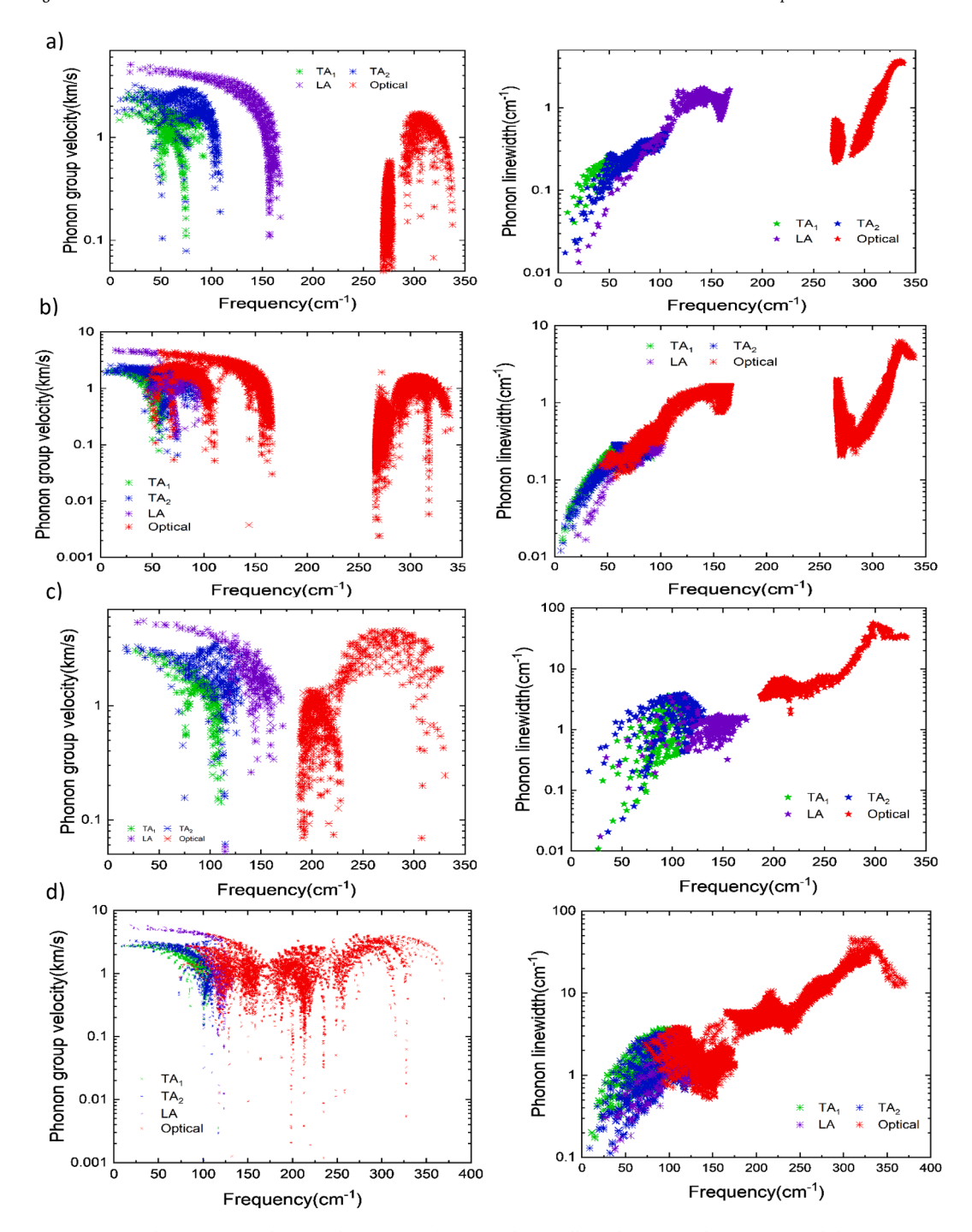


Fig. 5. Mode contribution thermal conductivity of MgSe at 300 K for different crystalline phase.

temperature respectively. λ represents the vibrational mode (qj) (q is the wave vector and j represent phonon polarization). $\omega_{\lambda}, \overline{n}_{\lambda}$, and $\nu_{\alpha\lambda}$ $(= \partial \omega_{\lambda}/\partial q)$ are the phonon frequency, equilibrium Bose-Einstein population and group velocity along cartesian direction α , respectively of a phonon mode λ . $\omega_{\lambda}, \overline{n}_{\lambda}$, and $c_{\alpha\lambda}$ are derived from the knowledge of phonon

dispersion computed using 2nd order IFCs. τ_{λ} is the phonon lifetime and is computed using the equation,



 $\textbf{Fig. 6.} \ \ \textbf{Phonon group velocity and scattering of MgSe with crystalline phase; a) ZB b) WZ c) RS \ and \ d) \ NiAs. \\$

$$\frac{1}{\tau_{\lambda}} = \pi \sum_{\lambda \lambda''} |V_{3}(-\lambda, \lambda', \lambda'')|^{2} \times [2(n_{\lambda'} - n_{\lambda''})\delta(\omega(\lambda) + \omega(\lambda') - \omega(\lambda'')) + (1 + n_{\lambda''} + n_{\lambda''})\delta(\omega(\lambda) - \omega(\lambda') - \omega(\lambda''))]$$
(2)

where, $\frac{1}{\tau_{i}}$ is the anharmonic scattering rate based on the lowest order three phonon interactions and $V_3(-\lambda,\lambda^*,\lambda^{**})$ are the three-phonon coupling matrix elements computed using both harmonic (2nd order) and anharmonic (3rd order) interatomic force constants. 2nd and 3rd order interatomic force constants were derived from density-functional perturbation theory (DFPT) [43,44]. Harmonic force constants were computed on an $8\times8\times8$ q-grid for ZB and RS systems and on a $9\times9\times$

6 grid for WZ and NiAs structures. Anharmonic force constants were computed on a 4 \times 4 \times 4 grid for ZB and RS and on a 3 \times 3 \times 2 grid for WZ and NiAs structures, using D3Q [41,45,46] package within QUANTUM-ESPRESSO. Acoustic sum rules were imposed on both harmonic and anharmonic interatomic force constants. Phonon linewidth and lattice thermal conductivity were calculated using 'thermal2' package within QUANTUM ESPRESSO. For these calculations, q-mesh of $30\times30\times30$ was used for ZB and RS structures, while a mesh of $30\times30\times20$ was used for WZ and NiAs structures. Iterations in the exact solution of the PBTE were performed until Δk between consecutive iterations diminished to below $1.0e^{-5}$. k values were typically converged after 4 iterations. Casimir scattering [47] was imposed to include the effect of boundary scattering for computing length dependent thermal

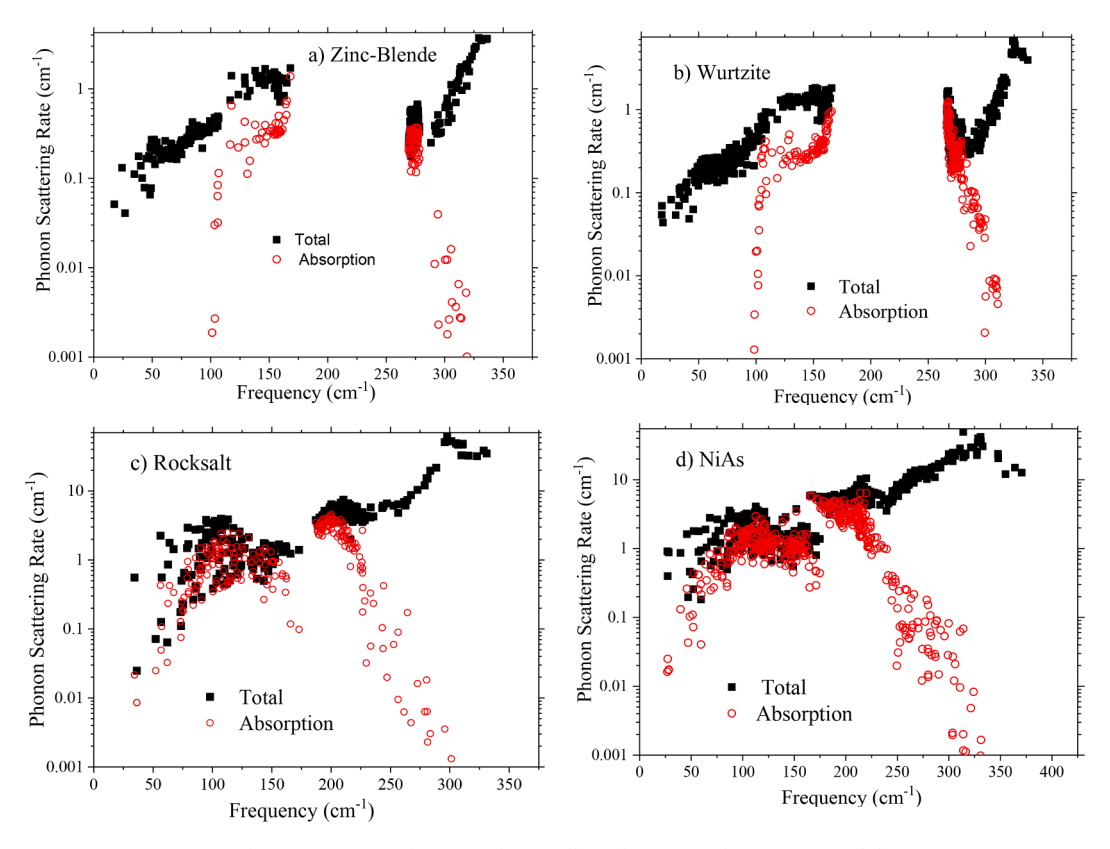


Fig. 7. Phonon scattering of MgSe with crystalline phase; a) ZB b) WZ c) RS and d) NiAs.

conductivity in the nanoscales. Phonon-isotope scattering is included for the effect of isotope variation with naturally occurring isotopes of Mg and Se [48]. Elastic constants were computed using QUANTUM ESPRESSO thermo_pw package. Voigt-Reuss-Hill approximation [49] was used to calculate Bulk modulus, Shear modulus (G), Young's Modulus (E) and Poisson's ratio (v).

3. Results and discussion

Phonon dispersion and phonon density of states (PDOS) for the MgSe with crystalline phases of ZB, WZ, RS and NiAs are shown in Fig. 2 a-d. Computed dispersions are in good agreement with previously reported values [14]. Elastic properties such as Young's modulus (E), Bulk modulus (B), Shear modulus (G) and Poisson's ratio based on Voigt-Ruess-Hill approximation are listed in Table 1 and are also in excellent agreement with the previously published work [14].

Lattice thermal conductivity (k) of MgSe for different crystalline phases is shown in Fig. 3a. Single-mode relaxation results (SMA) are 5% less than the iterative solution. At room temperature (300 K), computed k of pure MgSe is as follows; $k_{\rm NiAs}$ (4.54 Wm $^{-1}$ K $^{-1}$ along a-axis and 6.37 Wm $^{-1}$ K $^{-1}$ along c-axis) $< k_{\rm RS}$ (11.89 Wm $^{-1}$ K $^{-1}$) $< k_{\rm WZ}$ (19.58 Wm $^{-1}$ K $^{-1}$ along a-axis and 20.39 Wm $^{-1}$ K $^{-1}$ along c-axis) $< k_{\rm ZB}$ (21.27 Wm $^{-1}$ K $^{-1}$). Fig. 3b shows the length dependent thermal conductivity of MgSe between 10 nm and 10 μ m. At 300 K and at 100 nm, k of different crystalline phases are as follows; $k_{\rm NiAs}$ (3.25 Wm $^{-1}$ K $^{-1}$ along a-axis and 4.67 Wm $^{-1}$ K $^{-1}$ along c-axis) $< k_{\rm RS}$ (5.71 Wm $^{-1}$ K $^{-1}$) $< k_{\rm WZ}$ (8.05 Wm $^{-1}$ K $^{-1}$ aris and 8.76 Wm $^{-1}$ K $^{-1}$ along c-axis) $< k_{\rm ZB}$ (8.82 Wm $^{-1}$ K $^{-1}$).

Lattice thermal conductivity of naturally occurring MgSe, which includes the effect of isotopic disorder is shown in Fig. 4. Thermal conductivity of naturally occurring MgSe at 300 K is as follows; $k_{\rm NiAs}$ (4.36 Wm⁻¹K⁻¹ along a-axis and 6.13 Wm⁻¹K⁻¹ along c-axis) $< k_{\rm RS}$ (11.31 Wm⁻¹K⁻¹) $< k_{\rm WZ}$ (17.5 Wm⁻¹K⁻¹ a-axis and 18.3 Wm⁻¹K⁻¹ along c-axis) $< k_{\rm ZB}$ (19.04 Wm⁻¹K⁻¹). These values show that isotopic scattering reduces its lattice thermal conductivity by a maximum of \sim

10% for ZB and WZ phase.

As seen above, thermal conductivity of the NiAs crystal phase is the lowest, while that of zincblende phase is the highest. Thermal conductivity of MgSe with zincblende crystal structure is 4.68 times that of the NiAs phase along a-axis. In Fig. 5, we also compare contributions of different vibration modes to overall thermal conductivity in different crystalline phases. Interestingly, in NiAs and wurtzite MgSe, k contribution from optical phonon is higher than the acoustic phonon modes.

This is mainly due to the suppression of phonon–phonon scattering in zincblende structure mediated by a large phonon bandgap ($\sim 100~\text{cm}^{-1}$) in the phonon dispersion of zinc-blende structure. We have presented the phonon scattering rates (inverse of phonon lifetime) and phonon group velocities of MgSe with different crystalline phases in Fig. 6. We can observe from Fig. 6a and d that, scattering rate of TA₁ and TA₂ for NiAs is approximately one order of magnitude higher than that of the zincblende phase causing a dramatic reduction in thermal conductivity contributions of TA₁ and TA₂ phonon modes in NiAs structure.

The effect can be understood by observing that anharmonic scattering of phonons through the lowest-order three phonon processes can be classified into two categories - absorption scattering process, where a phonon mode $(q\omega)$ scatters by absorbing another phonon mode $(q'\omega')$, yielding a higher energy $(q''\omega'')$ phonon mode, and decay processes, where a phonon mode decays into two lower energy phonons. These processes satisfy energy and momentum conservation given by, $\omega+\omega'=\omega''$ (energy), q+q'=q'' (momentum) for absorption process and $\omega=\omega'+\omega''$ (energy), q=q'+q'' (momentum) for decay process.

The large energy gap in the phonon dispersion of ZB structure suppresses the absorption scattering channels for acoustic phonons involving scattering of an acoustic phonon by absorbing another acoustic phonon to convert into an optical phonon. The large energy gap in the phonon dispersion of the ZB structure prohibits energy conservation ($\omega + \omega' = \omega''$) for such absorption scattering channels. This is seen through an example, where, an acoustic phonon of frequency 100 cm^{-1} cannot scatter into an optical phonon, even by absorbing the highest

frequency acoustic phonon ($168.05~{\rm cm}^{-1}$). This is because the lowest optical phonon frequency $269.25~{\rm cm}^{-1}$ is higher than the sum of the frequencies of above two listed acoustic phonons. This elimination of absorption scattering channels in ZB structure dramatically decreases overall scattering rates in ZB case. We have shown this for all crystalline phases in Fig. 7. where we compare the magnitude of absorption scattering channel with the overall scattering rates.

It can be seen that for ZB and WZ structures (with a large bandgap in their phonon dispersions), the magnitude of absorption channels is significantly smaller than for the case of RS and NiAs structures. Below a frequency of $100~{\rm cm}^{-1}$, the absorption channel is seen to be almost completely absent in ZB and WZ structures. This smaller rate of absorption scattering in ZB and WZ structures also leads to a smaller overall scattering rate in these structures. At a frequency of $50~{\rm cm}^{-1}$, the overall scattering rate in ZB and WZ structures is $\sim 0.1~{\rm cm}^{-1}$, almost an order of magnitude lower, relative to the scattering rate of $1~{\rm cm}^{-1}$ in NiAs structure. The higher scattering rates in RS and NiAs structures (due to smaller or absent phonon band gap) lead to lower thermal conductivity in these crystalline phases.

Higher contribution of optical phonon modes to overall thermal conductivity in NiAs and WZ structures can now be understood in terms of the phonon band gap in these materials. In NiAs structure, the large scattering rates of acoustic phonons (due to absence of a band gap in phonon dispersion), imply that the scattering rates of low frequency optical phonons become comparable to that of acoustic phonons. Significant group velocities of optical phonons in NiAs structure combined with comparable phonon scattering rates to acoustic phonons, leads to high thermal conductivity contribution of optical phonons in NiAs structure. In WZ crystalline phase, the high thermal conductivity of optical phonons arises due to the large phonon band gap in the dispersion. Fig. shows that some of the optical phonons are below the band gap. Similar to the case of acoustic phonons, these optical phonons also experience inhibited scattering from optical phonons above the band gap

4. Conclusion

In this work, thermal conductivity of magnesium selenide (MgSe) with four crystalline phases; zincblende, rocksalt, wurtzite and nickel arsenic were computed by first principles calculations with phonon Boltzmann transport equations. Our first principles calculations shows a low thermal conductivity of less than $\sim 20~{\rm Wm^{-1}K^{-1}}$ for all the crystalline phase of MgSe. Isotopic disorder scattering has minimal effect (less than 10%) to its overall thermal conductivity. We systematically investigated the phonon group velocity, phonon scattering rate and mode dependent thermal conductivity of MgSe. Our first principles calculations shows that, NiAs and wurtzite has significant contributions from optical phonons than NiAs and rocksalt. At nanometer length scales such as 100 nm, thermal conductivity of less than 3.25 ${\rm Wm^{-1}K^{-1}}$ for MgSe with NiAs crystalline phase shows a promising nature of MgSe for thermoelectric applications.

5. Data availability

The raw/processed data required to reproduce these findings can be shared upon request.

CRediT authorship contribution statement

Rajmohan Muthaiah: Conceptualization, Methodology, Data curation, Writing - original draft. **Jivtesh Garg:** Software, Supervision, Validation, Funding acquisition, Writing - original draft, Writing - review & editing.

Declaration of Competing Interest

The authors declare that they have no known competing financial interests or personal relationships that could have appeared to influence the work reported in this paper.

Acknowledgements

R.M and J.G would like to acknowledge OU Supercomputing Center for Education Research (OSCER) for providing computational resources. J.G and R.M acknowledge financial support from NSF CAREER grant, Award # 1847129.

References

- [1] B.J. Baliga, in: Wide Bandgap Semiconductor Power Devices, Elsevier, 2019, pp. 1–19, https://doi.org/10.1016/B978-0-08-102306-8.00001-0.
- [2] M.A. di Forte-Poisson, M. Magis, M. Tordjmann, J. di Persio, Chapter 5 MOCVD Growth of Group III Nitrides for High-power, High-frequency Applications, in: M. Razeghi, M. Henini (Eds.), Optoelectronic Devices: III Nitrides, Elsevier, Oxford, 2005, pp. 69–94.
- [3] J. Millán, P. Godignon, Wide Band Gap power semiconductor devices, in: 2013 Spanish Conference on Electron Devices, 2013, pp. 293–296.
- [4] Y.u. Xiao, L.-D. Zhao, Seeking new, highly effective thermoelectrics, Science 367 (6483) (2020) 1196–1197.
- [5] B. Kucukgok, Thermoelectric phenomena for waste heat harvesting using wide bandgap semiconductors, The University of North Carolina at Charlotte, 2015.
- [6] B. Kucukgok, Q. He, A. Carlson, A.G. Melton, I.T. Ferguson, N. Lu, Investigation of Wide Bandgap Semiconductors for Thermoelectric Applications, MRS Proceedings 1490 (2013) 161–166.
- [7] M.-L. Liu, F.-Q. Huang, L.-D. Chen, I.-W. Chen, A wide-band-gap p-type thermoelectric material based on quaternary chalcogenides of Cu2ZnSnQ4 (Q=S, Se), Appl. Phys. Lett. 94 (20) (2009) 202103, https://doi.org/10.1063/1.3130718.
- [8] F. Drief, A. Tadjer, D. Mesri, H. Aourag, First principles study of structural, electronic, elastic and optical properties of MgS, MgSe and MgTe. *Catalysis Today* 89 (3) (2004) 343–355.
- [9] M. Sajjad, H.X. Zhang, N.A. Noor, S.M. Alay-e-Abbas, M. Younas, M. Abid, A. Shaukat, Theoretical Investigation of Structural, Electronic, and Magnetic Properties of V-Doped MgSe and MgTe Semiconductors, J. Supercond. Novel Magn. 27 (10) (2014) 2327–2336.
- [10] D. Rached, N. Benkhettou, B. Soudini, B. Abbar, N. Sekkal, M. Driz, Electronic structure calculations of magnesium chalcogenides MgS and MgSe, Physica Status Solidi (B) 240 (3) (2003) 565–573.
- [11] S.-G. Lee, K.J. Chang, First-principles study of the structural properties of MgS-, MgSe-, ZnS-, and ZnSe-based superlattices, Phys. Rev. B 52 (3) (1995) 1918–1925.
- [12] S.G. Parker, A.R. Reinberg, J.E. Pinnell, W.C. Holton, Preparation and Properties of Mg[sub x]Zn[sub 1-x]Te, J. Electrochem. Soc. 118 (6) (1971) 979, https://doi. org/10.1149/1.2408236.
- [13] A. Kuhn, A. Chevy, M.-J. Naud, Preparation and some physical properties of magnesium telluride single crystals, J. Cryst. Growth 9 (1971) 263–265.
- [14] S. Duman, S. Bağcı, H.M. Tütüncü, G.P. Srivastava, First-principles studies of ground-state and dynamical properties of MgS, MgSe, and MgTe in the rocksalt, zinc blende, wurtzite, and nickel arsenide phases, Phys. Rev. B 73 (20) (2006), 205201
- [15] G. Gökoğlu, First principles vibrational dynamics of magnesium telluride, J. Phys. Chem. Solids 71 (9) (2010) 1388–1392.
- [16] F. Zhang, C. Chen, H. Yao, F. Bai, L.i. Yin, X. Li, S. Li, W. Xue, Y. Wang, F. Cao, X. Liu, J. Sui, Q. Zhang, High-Performance N-type Mg3Sb2 towards Thermoelectric Application near Room Temperature, Adv. Funct. Mater. 30 (5) (2020) 1906143, https://doi.org/10.1002/adfm.v30.510.1002/adfm.201906143.
- [17] J. Li, S. Zheng, T. Fang, L. Yue, S. Zhang, G. Lu, Computational prediction of a high ZT of n-type Mg3Sb2-based compounds with isotropic thermoelectric conduction performance, PCCP 20 (11) (2018) 7686–7693.
- [18] A.V. Dmitriev, High doping effect on the thermoelectric properties of p-type lead telluride, J. Appl. Phys. 123 (16) (2018) 165707, https://doi.org/10.1063/ 1.5025766.
- [19] J. Zhang, L. Song, S.H. Pedersen, H. Yin, L.T. Hung, B.B. Iversen, Discovery of high-performance low-cost n-type Mg3Sb2-based thermoelectric materials with multivalley conduction bands, Nat. Commun. 8 (1) (2017) 13901.
- [20] Z.H. Dughaish, Lead telluride as a thermoelectric material for thermoelectric power generation, Phys. B 322 (1-2) (2002) 205–223.
- [21] A. Waag, H. Heinke, S. Scholl, C.R. Becker, G. Landwehr, Growth of MgTe and Cd1-xMgxTe thin films by molecular beam epitaxy, J. Cryst. Growth 131 (3-4) (1993) 607-611.
- [22] F. Tarannum, R. Muthaiah, R.S. Annam, T. Gu, J. Garg, Effect of Alignment on Enhancement of Thermal Conductivity of Polyethylene-Graphene Nanocomposites and Comparison with Effective Medium Theory, Nanomaterials 10 (7) (2020) 1291.
- [23] R. Muthaiah, F. Tarannum, R.S. Annam, A.S. Nayal, S. Danayat, J. Garg, Thermal conductivity of hexagonal BC2P – a first-principles study, RSC Adv. 10 (70) (2020) 42628–42632.

- [24] R. Muthaiah, J. Garg, Strain tuned high thermal conductivity in boron phosphide at nanometer length scales – a first-principles study, PCCP 22 (36) (2020) 20914–20921.
- [25] A. Shafique, Y.-H. Shin, Ultrahigh and anisotropic thermal transport in the hybridized monolayer (BC2N) of boron nitride and graphene: a first-principles study, PCCP 21 (31) (2019) 17306–17313.
- [26] R. Muthaiah, J. Garg, Temperature effects in the thermal conductivity of aligned amorphous polyethylene—A molecular dynamics study, J. Appl. Phys. 124 (10) (2018) 105102, https://doi.org/10.1063/1.5041000.
- [27] L. Lindsay, D.A. Broido, T.L. Reinecke, Ab initio thermal transport in compound semiconductors, Physical Review B 87 (16) (2013), 165201.
- [28] S.K. Oh, J.S. Lundh, S. Shervin, B. Chatterjee, D.K. Lee, S. Choi, J.S. Kwak, J.-H. Ryou, Thermal Management and Characterization of High-Power Wide-Bandgap Semiconductor Electronic and Photonic Devices in Automotive Applications, J. Electron. Package 141 (2) (2019).
- [29] J.G. Thakare, C. Pandey, M.M. Mahapatra, R.S. Mulik, Thermal Barrier Coatings—A State of the Art Review, Met. Mater. Int. (2020).
- [30] D.R. Clarke, S.R. Phillpot, Thermal barrier coating materials, Mater. Today 8 (6) (2005) 22–29.
- [31] N.P. Padture, M. Gell, E.H. Jordan, Thermal Barrier Coatings for Gas-Turbine Engine Applications, Science 296 (5566) (2002) 280–284.
- [32] B.M. Basol, B. McCandless, Brief review of cadmium telluride-based photovoltaic technologies, J. Photonics Energy 4 (1) (2014) 040996, https://doi.org/10.1117/ 1. IPF 4.040996
- [33] M. Saadah, Thermal Management of Solar Cells, 2013.
- [34] K. Zweibel, The Impact of Tellurium Supply on Cadmium Telluride Photovoltaics, Science 328 (5979) (2010) 699–701.
- [35] P. Giannozzi, S. Baroni, N. Bonini, M. Calandra, R. Car, C. Cavazzoni, D. Ceresoli, G.L. Chiarotti, M. Cococcioni, I. Dabo, A. Dal Corso, S. de Gironcoli, S. Fabris, G. Fratesi, R. Gebauer, U. Gerstmann, C. Gougoussis, A. Kokalj, M. Lazzeri,
 - L. Martin-Samos, N. Marzari, F. Mauri, R. Mazzarello, S. Paolini, A. Pasquarello, L. Paulatto, C. Sbraccia, S. Scandolo, G. Sclauzero, A.P. Seitsonen, A. Smogunov,
 - P. Umari, R.M. Wentzcovitch, QUANTUM ESPRESSO: a modular and open-source

- software project for quantum simulations of materials, J. Phys.: Condens. Matter 21 (39) (2009), 395502.
- [36] D.M. Ceperley, B.J. Alder, Ground State of the Electron Gas by a Stochastic Method, Phys. Rev. Lett. 45 (7) (1980) 566–569.
- [37] H.J. Monkhorst, J.D. Pack, Special points for Brillouin-zone integrations, Phys. Rev. B 13 (12) (1976) 5188–5192.
- [38] A. Chakrabarti, Role of NiAs phase in pressure-induced structural phase transitions in IIA-VI chalcogenides, Phys. Rev. B 62 (3) (2000) 1806–1814.
- [39] P.E. Van Camp, V.E. Van Doren, J.L. Martins, High-pressure phases of magnesium selenide and magnesium telluride, Phys. Rev. B 55 (2) (1997) 775–779.
- [40] H. Okuyama, K. Nakano, T. Miyajima, K. Akimoto, Epitaxial growth of ZnMgSSe on GaAs substrate by molecular beam epitaxy, J. Cryst. Growth 117 (1-4) (1992)
- [41] G. Fugallo, M. Lazzeri, L. Paulatto, F. Mauri, Ab initio variational approach for evaluating lattice thermal conductivity, Phys. Rev. B 88 (4) (2013), 045430.
- [42] G.P. Srivastava, The physics of phonons, 2019.
- [43] A. Debernardi, S. Baroni, E. Molinari, Anharmonic Phonon Lifetimes in Semiconductors from Density-Functional Perturbation Theory, Phys. Rev. Lett. 75 (9) (1995) 1819–1822.
- [44] G. Deinzer, G. Birner, D. Strauch, Ab initio calculation of the linewidth of various phonon modes in germanium and silicon, Phys. Rev. B 67 (14) (2003), 144304.
- [45] L. Paulatto, I. Errea, M. Calandra, F. Mauri, First-principles calculations of phonon frequencies, lifetimes, and spectral functions from weak to strong anharmonicity: The example of palladium hydrides, Phys. Rev. B 91 (5) (2015), 054304.
- [46] L. Paulatto, F. Mauri, M. Lazzeri, Anharmonic properties from a generalized thirdorder ab initio approach: Theory and applications to graphite and graphene, Phys. Rev. B 87 (21) (2013), 214303.
- [47] H.B.G. Casimir, Note on the conduction of heat in crystals, Physica 5 (6) (1938) 495–500.
- [48] T.B. Coplen, Atomic Weights of the Elements 1995, J. Phys. Chem. Ref. Data 26 (5) (1997) 1239–1253.
- [49] D.H. Chung, W.R. Buessem, The Voigt-Reuss-Hill (VRH) Approximation and the Elastic Moduli of Polycrystalline ZnO, TiO2 (Rutile), and α -Al2O3, J. Appl. Phys. 39 (6) (1968) 2777–2782.